Proceedings of the 21st ICSMGE, Vienna, Austria, 14 – 19 June 2026. Pistrol, Adam & Schweiger (eds.)
Published by: ÖGG, Austrian Society for Geomechanics, Salzburg, Austria, ISBN 978-3-9503898-4-5
https://doi.org/10.53243/ICSMGE2026-680

Mesh Dependency and Shear Banding in Finite Element Modeling of Silty Sands: Challenges and Solutions

Mazdak Atri, Tim Pucker
Department of Civil Engineering, HafenCity University Hamburg, Germany, mazdak.atri@hcu-hamburg.de

ABSTRACT: Shear banding, the localized deformation that occurs in soils near peak stress, is a critical phenomenon in geotechnical engineering, influencing various challenges such as slope stability, foundation performance, and the failure mechanisms of geotechnical structures. Since natural soils are often mixtures of different materials, understanding the shear behavior of mixed soils is essential. In this study, the finite element modeling of silty sands is investigated to assess their shear behavior under elastoplastic conditions. When applying the finite element method and elastoplastic modeling of silty sands, the formation of shear bands reveals a significant influence on the finite element mesh. The mesh size affects the shear band thickness and shear strength of the simulations. With mesh analysis, it is revealed that the shear behavior changes, and there is no mesh convergence. This leads to simulation results that could deviate significantly from observed or expected real-world behavior. This paper documents investigations into mesh dependency in the modeling of silty sands using the finite element method. The focus is on the influence of mesh size and its effect on the representation of local shear bands. Recommendations are developed on how to address this phenomenon in practice and which alternative approaches can reduce this mesh dependency.

KEYWORDS: Shear banding, mesh dependency, finite element modeling, silty sand, strain localization

1 INTRODUCTION AND BACKGROUND

Shear banding, which involves the formation of narrow zones of highly localized deformation, is a crucial phenomenon governing failure mechanisms in geotechnical structures like slopes, foundations, and earth-retaining systems. This localized deformation typically begins near the peak soil stress and greatly affects the post-peak mechanical response (Desrues and Viggiani, 2004; Tatsuoka et al., 1990). Experimental results from plane strain and triaxial tests show that shear band development depends on stress conditions, relative density, particle size distribution, and fabric anisotropy (Han and Drescher, 1993; Chu et al., 1996; Alshibli and Sture, 1999). Shear band inclinations generally range from 50° to 65°, while band thickness usually falls between 7 and 20 times the mean grain diameter d_{50} (Finno et al., 1996; Oda et al., 1998; Lade et al., 2008).

Silty sands are especially important in this context because of their complex mechanical behavior, which combines the structural effects of granular materials with the influence of finer particles. Previous studies have shown that strain localization patterns in silty sands are highly sensitive to the material's gradation, particle shape, and initial density (Tang et al., 2018; Alshibli and Hasan, 2008). Therefore, understanding the shear behavior of silty sands is crucial for assessing the stability and performance of geotechnical structures that involve these materials.

While significant progress has been made in understanding shear banding through laboratory testing, numerical modeling of this phenomenon remains challenging. Classical finite element approaches based on Cauchy continua and local elastoplastic constitutive laws lack an internal length scale, meaning the material response at a point depends solely on local variables like stress and strain, without considering interactions with neighboring points. This limitation prevents the accurate representation of the physical width of shear bands and leads to mesh-dependent results. Furthermore, when strain localization occurs, the governing differential equations transition from elliptic to hyperbolic type, rendering the boundary value problem ill-posed (Ehlers et al., 2001; Stefanou and Gerolymatou, 2019). As a result, post-peak behavior and shear band characteristics become artifacts of the numerical discretization rather than true material properties.

This well-documented problem, known as mesh dependency, limits the reliability of classical FEM in capturing strain localization accurately. Additionally, previous research has shown that the formation and evolution of shear bands in numerical models are not only influenced by mesh density but are also significantly affected by boundary conditions. Constraints such as fixed or roller boundaries, loading type (displacement or force control), and specimen aspect ratio have a direct impact on the stress distribution, the initiation of strain localization, and the inclination or position of shear bands (Chu et al., 1996; Du et al., 2011; Alshibli and Hasan, 2008). Rigid boundary conditions may suppress natural deformation modes or promote artificial stress concentrations, further amplifying mesh sensitivity.

Various regularization techniques, such as viscosity-based models, nonlocal theories, high-order gradient models, and micropolar theories, have been proposed to address the mesh dependency issue (Liu et al., 2022). Among these, micropolar theory offers a strong physical basis for granular materials by incorporating couple stresses and micro-rotations related to grain-scale interactions. However, implementing such regularization is beyond the scope of this study.

This paper focuses on explicitly demonstrating the mesh dependency phenomenon in the finite element modeling of silty sands using a classical elastoplastic framework. The material behavior is represented by the linear elastic-plastic model with the Mohr-Coulomb failure criterion, which captures the frictional and cohesive strength parameters of silty sands under plane strain conditions. The objective is to quantify how mesh refinement and boundary conditions affect shear band formation, shear band thickness, and the stress-strain response. Rather than examining a range of sand-silt mixtures, this study uses a single representative silty sand to isolate and clearly illustrate the numerical effects of strain localization. To ensure that the results remain relevant and realistic, the material parameters are chosen based on values reported in the literature for typical silty sands. Additionally, this study aims to provide practical recommendations for interpreting FEM results involving strain localization when no regularization is applied.

2 NUMERICAL MODELING

2.1 *Material Model and Material Parameters*

The silty sand behavior is modeled using classical elastoplasticity with the Mohr-Coulomb failure criterion. This model captures the shear strength of soils based on the friction angle and cohesion, while the elastic behavior is governed by Young's modulus and Poisson's ratio.

Parameters such as the critical state friction angle φ_c, peak friction angle φ_p, and dilatancy angle ψ control the shear strength, dilation behavior, and strain localization tendencies of the material. Inaccurate parameter selection can lead to misleading simulation results and unsafe or overly conservative designs. To address this, Salgado et al. (2000) proposed a semi-empirical framework to estimate these parameters based on drained triaxial compression tests on silty sands.

The study by Salgado et al. (2000) used Ottawa sand mixed with varying amounts (0 - 20%) of non-plastic Georgia silt. The core of the method is the calculation of the dilatancy index I_R, given by Equation (1).

$$I_R = I_D \left(Q - \ln\left(\frac{100 p_p'}{P_A} \right) \right) - R \qquad (1)$$

where I_D is the relative density, Q and R are empirical parameters dependent on fines content, p_p' is the mean effective stress at peak strength, and P_A = 100 kPa is atmospheric pressure. Once I_R is known, the peak friction angle and dilatancy angle can be estimated using the empirical relationships developed by Bolton (1986):

$$\varphi_p = \varphi_c + 3I_R, \qquad \psi = \frac{\varphi_p - \varphi_c}{0.8} \qquad (2)$$

The Table 1 presents the estimated values of φ_c, φ_p, and ψ for different fines contents at a relative density of 80% and a confining pressure of 100 kPa, using this method.

Table 1. Estimated φ_c, φ_p, and ψ (Dr = 80%)

Fines Content (%)	φ_c (°)	φ_p (°)	ψ (°)
0	29.0	36.47	9.34
5	30.5	40.64	12.67
10	32.0	40.96	11.20
15	32.5	42.87	12.96
20	33.0	41.53	10.66

The simulations employ the Mohr-Coulomb criterion in two forms: ideal plasticity (no hardening) and isotropic linear hardening with a modulus of $H = 200$ kPa. The material represents a silty sand with 10% fines content, a typical natural soil configuration. The parameters are characteristic of dense silty sands with this fines content and are summarized in Table 2.

Table 2. Material parameters for the Mohr-Coulomb model.

Parameter	Symbol	Value	Unit
Young's modulus	E	60	MPa
Poisson's ratio	v	0.3	-
Friction angle	φ_c	32.0	°
Cohesion	c	1	kPa
Dilation angle	ψ	11.20	°

These parameters are kept constant in all simulations to isolate the effects of mesh refinement and boundary conditions on the mechanical response and the development of shear bands.

2.2 *Geometry and Boundary Conditions*

The numerical model simulates a confined plane strain compression test, a common approach for investigating strain localization and shear band formation in silty sand. Under the plane strain assumption, out-of-plane strains are constrained to zero while out-of-plane stresses are allowed to develop, replicating conditions typically used in laboratory testing.

The modeled geometry represents one-quarter of a rectangular soil specimen with dimensions of 2.5 cm in width and 5 cm in height. Symmetry is applied along both horizontal and vertical axes to reduce computational cost while preserving the essential deformation behavior.

Two boundary condition configurations are considered to examine the influence of shear band formation in plane strain:

- **(a) No-shear configuration:** The left boundary is fixed in the horizontal direction (u_1 = 0), and the bottom boundary is fixed in the vertical direction (u_2 = 0), consistent with symmetry. The top boundary is left unconstrained in both directions. This setup suppresses shear strain and is used for verifying the numerical results against an analytical solution without shear localization.
- **(b) Shear-permitting configuration**: As in case (a), the left and bottom boundaries are constrained due to symmetry. However, the top boundary is fixed in the horizontal direction (u_1 = 0), allowing vertical movement only. This boundary condition generates shear stress and facilitates the development of shear bands, making it suitable for studying post-peak behavior in silty sand (e.g., Arslan and Sture, 2008; Liu, 2018; Chang et al., 2021).

The loading is applied in two stages:

1. **Confinement Phase:** A uniform confining pressure of $\sigma_3' = 100$ kPa is applied on the right and top boundaries to replicate realistic confinement.
2. **Loading Phase:** A vertical displacement is prescribed at the top boundary, increasing linearly until 20 % axial strain is reached.

By comparing configurations (a) and (b), the study explores the role of shear band formation in the stress–strain response and evaluates the degree of mesh dependency in finite element simulations of silty sand (see Figure 1).

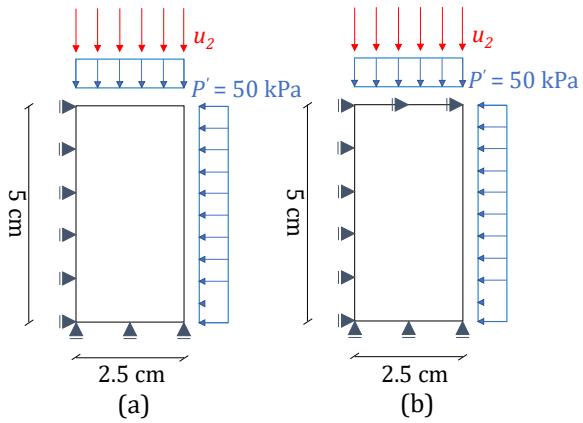

Figure 1. Boundary conditions: (a) no shear, for verification; (b) shear-permitting, for localization analysis.

2.3 *Mesh Design and Refinement*

The soil specimen is discretized using a structured quadrilateral mesh composed of four-node, full integration, plane strain elements (CPE4) available in Abaqus. To investigate the influence of mesh refinement on strain localization and stress response, three levels of mesh density are used.

The coarsest mesh contains 8 elements along the width and 16 elements along the height, resulting in an average element size of 3.125 mm. Medium and fine meshes are generated by progressively reducing the element size by approximately half at each refinement step, while maintaining the specimen's overall dimensions. This strategy enables a systematic assessment of how mesh density affects both stress–strain behavior and shear band development.

Mesh refinement is applied uniformly across the entire specimen to avoid bias or artificial localization due to uneven meshing. With geometry, boundary conditions, and loading kept constant across all mesh densities, the influence of mesh size on shear band formation, band thickness, and stress–strain response can be consistently evaluated. An overview of the mesh configurations is provided in Table 3.

Table 3. Mesh configurations used in the simulations

Mesh Level	Elements (W × H)	Number of Elements	Element size (mm)
Coarse	*8 × 16*	128	3.125
Medium	*(8 × 2) × (16 × 2)*	512	1.5625
Fine	*(8 × 4) × (16 × 4)*	2048	0.78125

2.4 *Post-Processing and Evaluation Metrics*

Post-processing focuses on evaluating how mesh refinement influences the mechanical response and the development of shear bands in confined plane strain compression simulations. The force-displacement response is extracted by recording the reaction force at the top boundary and plotting it against the applied vertical displacement. This provides a basis for comparing the mechanical behavior across different mesh densities.

Shear band development is examined through contour plots of plastic shear strain at selected stages of loading. These plots are used to assess shear band characteristics, including inclination angle and thickness.

Shear band inclination is estimated by identifying the dominant orientation of the localized plastic strain zones relative to the horizontal axis. Shear band thickness is measured by evaluating the width of these zones. Comparisons across mesh levels allow for a direct assessment of mesh dependency.

3 RESULTS AND DISCUSSION

3.1 *Model Verification*

To validate the numerical model, simulations were performed using the Mohr-Coulomb constitutive law with ideal plasticity under the no-shear boundary condition (Figure 1a). This setup prevents strain localization, enabling a direct comparison between the numerical results and analytical predictions for plane strain compression of silty sand.

The vertical stress-strain response was computed for various mesh densities using Abaqus. Figure 2 presents the comparison of axial stress σ_1 versus axial strain ε_1 for the numerical models alongside the analytical solution. In the analytical solution, the axial stress in the elastic regime is given by the plane strain expression shown in Equation (3).

$$\sigma_1 = \frac{E}{1-\nu^2}\cdot\varepsilon_1 + \frac{\nu(1+\nu)}{1-\nu^2}\cdot\sigma_3 \qquad (3)$$

where σ_1 is the axial (vertical) stress, ε_1 is the axial strain, σ_3 is the confining pressure applied horizontally, E is Young's modulus, and ν is Poisson's ratio.

Plastic yielding is assumed to occur once the axial stress reaches the Mohr-Coulomb yield stress, as defined by Equation (4).

$$\sigma_1^{yield} = \sigma_3 \cdot \frac{1+\sin\varphi}{1-\sin\varphi} - \frac{2c\cdot\cos\varphi}{1-\sin\varphi} \qquad (4)$$

where φ is the internal friction angle and c is the cohesion of the material.

In the Mohr-Coulomb model, cohesion can be considered as a parameter that governs plastic hardening or softening behavior. However, in the case of ideal plasticity used here, cohesion remains constant throughout the deformation process, representing a perfectly plastic response without any post-yield evolution.

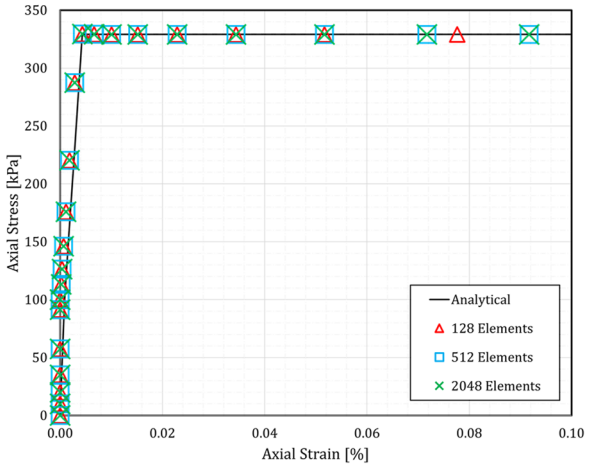

Figure 2. Numerical vs. analytical axial stress-strain curves under no-shear conditions.

The comparison demonstrates that the numerical results converge to the analytical solution in both the elastic and plastic regimes, regardless of mesh size. This confirms the correctness of the implementation in the absence of strain localization and provides a reliable reference for evaluating the mesh dependency under localization-permitting conditions.

3.2 *Force-Displacement Response*

The mechanical response of the silty sand specimens under confined plane strain compression is presented through total force-displacement plots, which illustrate the global behavior of the material under different modeling assumptions and boundary conditions.

Figure 3 shows the results for the Mohr-Coulomb elastoplasticity with ideal plasticity (no hardening), while Figure 4 presents the results for the model with isotropic linear hardening. In both figures, results are shown for two boundary condition configurations: the no-shear case (Figure 1a) and the shear-permitting case (Figure 1b). For each setup, three mesh densities are considered: coarse (128 elements), medium (512 elements), and fine (2048 elements).

Each curve represents the total vertical force versus total vertical displacement of the full specimen, reconstructed from the symmetrical quarter model. The total force is computed by summing the vertical reaction forces at all nodes along the top boundary, and the displacement corresponds to the prescribed vertical movement of the top surface.

In all simulations, the elastic portion of the response is mesh-independent, with consistent initial slopes across all mesh densities and material models. This confirms that mesh sensitivity only becomes relevant in the post-yield regime, where strain localization develops.

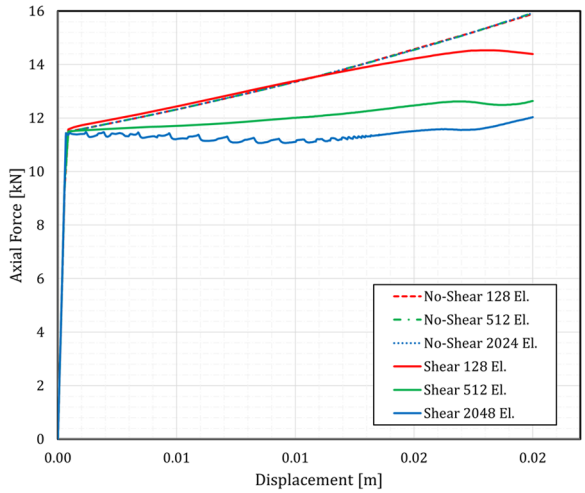

Figure 3. Force-displacement curves for ideal plasticity under no-shear and shear-permitting boundary conditions.

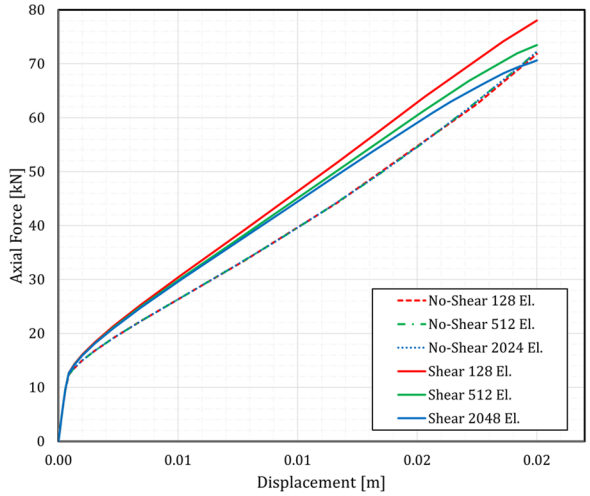

Figure 4. Force-displacement curves for linear hardening under no-shear and shear-permitting boundary conditions.

In both the ideal plastic and hardening models, when using the boundary condition that does not generate shear stress (no-shear case), the results remain stable and show clear mesh convergence. This indicates that in the absence of shear localization, the numerical solution is robust and reliable, even with coarse meshes.

After yielding, simulations with the shear-permitting boundary condition show that finer meshes result in lower total forces and more noticeable oscillations in the response. In contrast, coarser meshes produce higher force levels and smoother curves. This difference highlights how mesh resolution affects the development of strain localization and the redistribution of internal stresses when shear stresses are allowed to form.

Although adding isotropic linear hardening increases resistance to plastic deformation, it does not eliminate mesh dependency. It also helps reduce the amplitude of oscillations in the post-yield response, particularly in finer meshes. The numerical behavior becomes more stable, with fewer fluctuations, but the post-bifurcation force-displacement curves still vary with mesh refinement, resulting in an unrealistic numerical response that does not reflect a physical material behavior.

3.3 *Plastic Strain Localization*

The equivalent plastic strain (PEEQ) is a scalar measure used in finite element analysis to quantify the accumulated plastic deformation in a material. In Abaqus, it is computed from the plastic strain tensor and provides an effective way to visualize zones of intense plastic activity. The formulation is shown in Equation (5).

$$\bar{\varepsilon}^{pl} = \sqrt{\frac{2}{3}\varepsilon_{ij}^{p}\varepsilon_{ij}^{p}} \tag{5}$$

where ε_{ij}^{p} is the plastic strain tensor. This expression corresponds to the von Mises equivalent plastic strain, representing the magnitude of plastic strain energy in the material. PEEQ is particularly effective for identifying shear bands, as it integrates the entire history of plastic deformation and accumulates locally in zones of intense irreversible strain, providing a clear visual indicator of where strain localization occurs. These high-gradient zones in PEEQ contours typically align with observed shear bands in both numerical simulations and experimental observations. It is independent of the stress path and effectively reflects the accumulated plastic deformation throughout the loading history (Dassault Systèmes, 2024).

To examine the development of localized deformation, equivalent plastic strain (PEEQ) contours are plotted at 20% axial strain. Figure 5a shows the results for the Mohr-Coulomb model with ideal plasticity, while Figure 5b presents the results for the model with isotropic linear hardening. In each subfigure, contours are shown for three mesh densities: coarse, medium, and fine.

Under the selected shear-permitting boundary condition (Figure 1b), strain localization occurs in both models. In the case of ideal plasticity (Figure 5a), well-defined and sharply localized shear bands develop, and they become increasingly narrow with mesh refinement. Although this may appear to reflect improved resolution, the changing geometry of the localized zones across mesh sizes indicates that the results are not mesh objective.

For the isotropic hardening model (Figure 5b), strain localization also occurs and remains mesh-dependent, but the bands are less sharply defined compared to the ideal plasticity case. The plastic deformation is more distributed, resulting in broader PEEQ zones and a more gradual development of localization. This behavior is expected, as the increasing cohesion in the hardening model provides additional resistance to plastic strain accumulation. As a result, the maximum PEEQ values in the hardening case are significantly lower than those in the ideal plasticity model, which is consistent with the linear growth of cohesion with loading.

3.4 *Shear Band Characterization*

A representative PEEQ contour from the simulation with 512 elements and ideal plasticity is shown in Figure 6. The shear band's inclination angle and thickness are annotated directly on the figure. The inclination angles are measured relative to the horizontal axis, and the thickness is estimated from the visible width of the localized plastic strain zone.

To quantify the geometry of the shear band, the thickness is measured at two locations: the top corner (14.9 mm) and the bottom corner (18.3 mm). The average shear band thickness is calculated as the mean of these two measurements. Similarly, the shear band inclination is estimated by measuring the angles of the upper and lower boundaries of the band, 49.9° at the top and 54.7° at the bottom. The average of these two values is taken as the representative shear band angle.

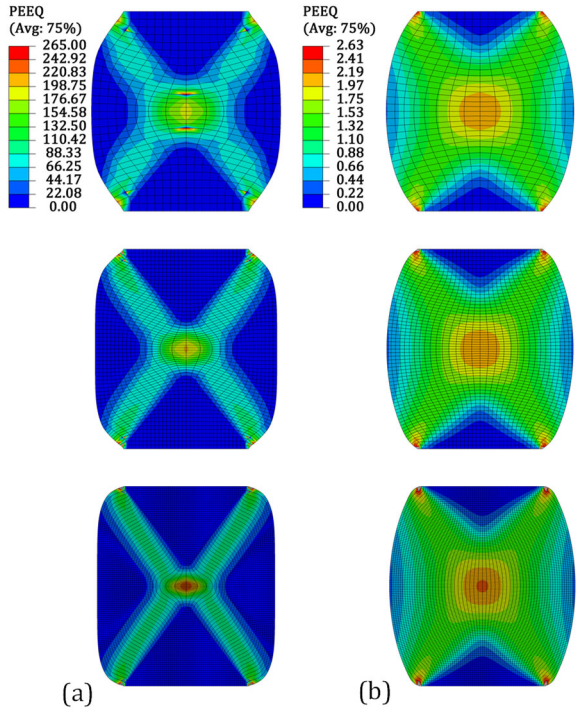

Figure 5. PEEQ contours at 20 % axial strain for (a) ideal plasticity and (b) isotropic linear hardening, shown from top to bottom for three mesh densities (128, 512, 2048 elements).

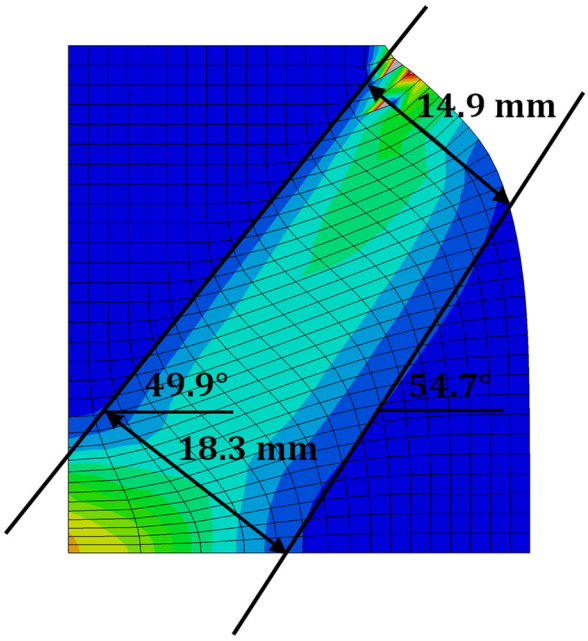

Figure 6. Shear band thickness and inclination in the 512-element ideal plastic model.

The measured shear band inclination angles and thicknesses across all mesh densities are summarized in Table 4. Overall, the average inclination angle shows a slight decreasing trend with mesh refinement. This behavior is more apparent in the isotropic hardening model, where the average angle gradually reduces from approximately 59.6° to 58.4°. In the ideal plasticity model, the angle also decreases consistently from coarse to medium meshes, dropping from 55.15° to 52.30°, and then slightly increasing to 54.15° at the finest mesh (2048 elements). This minor deviation at the finest resolution may be attributed to numerical instabilities and oscillations observed in the post-bifurcation response under ideal plasticity, which lacks the stabilizing effect of hardening.

Table 4. Shear band inclination and thickness across mesh densities.

Mesh Level	Material	Inclination (°)	Thickness (mm)
Coarse	Ideal Plastic	55.15	19.82
Medium	Ideal Plastic	52.30	16.60
Fine	Ideal Plastic	54.15	14.20
Coarse	Hardening	59.55	42.65
Medium	Hardening	58.90	40.65
Fine	Hardening	58.35	38.60

In terms of shear band thickness, both material models show a clear reduction with mesh refinement, reflecting the tendency of finer meshes to capture narrower localized plastic zones. However, the rate of reduction is notably different between the two models. In the ideal plasticity case, the average thickness decreases from 19.8 mm (128 elements) to 14.2 mm (2048 elements), indicating a sharp and consistent narrowing of the shear band. In contrast, the hardening model exhibits a more gradual reduction, with the average thickness decreasing from 42.7 mm to 38.6 mm over the same mesh range. This less behavior change highlights the effect of isotropic hardening in distributing plastic deformation more broadly, resulting in wider and more diffuse shear bands, even at higher mesh resolutions.

Together, these results reinforce the earlier observations from the PEEQ contours: while the orientation of the shear bands remains generally consistent and governed by the boundary conditions, band thickness is highly sensitive to mesh density, and this sensitivity is more pronounced in the absence of hardening.

4 CONCLUSIONS

This study investigated the strain localization behavior of a dense silty sand with 10% fines content using finite element simulations under confined plane strain compression. A linear elastoplastic constitutive model based on the Mohr-Coulomb failure criterion was used in two variants: one with ideal plasticity and the other incorporating isotropic linear hardening. The effect of mesh refinement was evaluated in terms of force-displacement response and shear band characteristics, including inclination and thickness. The focus of the study was not on the influence of different fines contents, but rather on characterizing the shear band formation behavior of a selected silty sand material.

The following key conclusions can be drawn:

- The numerical model was first verified using a no-shear boundary condition, where the results from the finite element simulations showed excellent agreement with the analytical solution. This confirmed that the model performs reliably in the absence of strain localization.
- The elastic portion of the force-displacement response was mesh independent in all simulations. The initial stiffness remained consistent across different mesh densities and material models, as expected from the linear elastic behavior.
- A comparison between the no-shear and shear-permitting boundary conditions demonstrated that mesh dependency only arises in the presence of strain localization, which is activated when shear bands form under shear-inducing boundary conditions.

- The post-bifurcation response was highly mesh sensitive in cases where shear bands developed. With mesh refinement, the force-displacement curves diverged significantly, showing no sign of mesh convergence, indicating that the localized deformation response is not objective.
- The addition of isotropic linear hardening reduced numerical oscillations and resulted in smoother force–displacement curves, especially in finer meshes. However, it did not eliminate mesh dependency, and both global and local responses continued to vary with mesh resolution. Compared to ideal plasticity, hardening led to more diffused shear bands and a more gradual development of localization.
- The thickness of the shear bands decreased clearly with mesh refinement in both material models. This effect was more pronounced in the ideal plasticity simulations, while the reduction was more gradual in the hardening case. The measurements confirm that band thickness is strongly controlled by mesh size and does not converge to an objective value.
- The inclination angle of the shear bands showed a slight decreasing trend with mesh refinement in both models. This trend was more apparent in the hardening model, while in the ideal plasticity case, some deviation appeared at the finest mesh, likely due to numerical instabilities.

5 OUTLOOK

The results of this study highlight the need for regularization to eliminate mesh dependency and achieve objective predictions of strain localization in silty sands. While some regularization approaches have been explored in the literature (Liu et al., 2022), there is still significant scope for further development and investigation across different classes of materials and failure mechanisms.

- **Cosserat continuum** or **micropolar models** introduce additional rotational degrees of freedom and couple stresses, which can lead to the emergence of a material length scale capable of regularizing shear band thickness and orientation. These models have shown potential in the context of granular materials, where interparticle rotations and contact mechanics influence strain localization. However, further implementation and systematic evaluation are needed to fully assess their effectiveness for different material models and different soils like silty sands.
- **Gradient-enhanced plasticity** and **nonlocal models** offer another avenue, where internal variables such as plastic strain are smoothed over a spatial neighborhood. These approaches may be more applicable to cohesive or partially cemented materials, but their broader potential and limitations for frictional granular soils still warrant investigation.

While some previous studies have applied Cosserat models to sands and silty sands with encouraging results, more comprehensive investigations are required. In particular, implementing Cosserat theory in combination with more advanced constitutive frameworks, such as complex elastoplastic models or hypoplastic models, could provide a better representation of the mechanical behavior of dense silty sands with fines, addressing the mesh dependency issue.

Future research will therefore focus on implementing and calibrating a micropolar plasticity and/or hypoplastic model for non-plastic granular materials, potentially using experimental data to estimate both classical and micropolar parameters. This direction could offer a path toward more physically meaningful and mesh-independent modeling of strain localization, with the potential to enhance predictive capabilities in geotechnical applications.

6 REFERENCES

Alshibli, K. and Hasan, A., 2008. Spatial variation of void ratio and shear band thickness in sand using X-ray computed tomography. *Géotechnique*, 58(4), 249–257.

Alshibli, K.A. and Sture, S. 1999. Sand shear band thickness measurements by digital imaging techniques. *Journal of Computing in Civil Engineering*, 13(2), 103–109.

Arslan, H. & Sture, S., 2008b. Finite element analysis of localization and micro–macro structure relation in granular materials. Part II: Implementation and simulations. *Acta Mechanica*, 197, 153–171.

Bolton, M.D., 1986. The strength and dilatancy of sands. *Géotechnique*, 36(1), 65–78.

Chang, J., Li, S., Wang, W. & Niu, Q., 2021. A study of non-coaxial effects on strain localization via micropolar plasticity model. *Acta Geotechnica*, 1–19.

Chu, J., Lo, S.C.R. and Lee, I.K. 1996. Strain softening and shear band formation of sand in multi-axial testing. *Géotechnique*, 46(1), 63–82.

Dassault Systèmes: *Abaqus 2024 Documentation*. Providence, RI: Dassault Systèmes Simulia Corp., 2024.

Desrues, J., and Viggiani, G. 2004. Strain localization in sand: an overview of the experimental results obtained in Grenoble using stereophotogrammetry. *International Journal for Numerical and Analytical Methods in Geomechanics*, 28(4), 279–321.

Du, X.L., Hou, S.W., Lu, D.C. and Cheng, X.L., 2011. Shear band analysis of sand based on digital image processing technique. *Advanced Materials Research*, 243, 2670–2678.

Ehlers, W. and Volk, W., 1997. On shear band localization phenomena of liquid-saturated granular elastoplastic porous solid materials accounting for fluid viscosity and micropolar solid rotations. *Mechanics of Cohesive-frictional Materials*, 2(4), 301–320.

Finno, R.J., Harris, W.W., Mooney, M.A. and Viggiani, G. 1996. Strain localization and undrained steady state of sand. *Journal of Geotechnical Engineering*, 122(6), 462–473.

Han, C. and Drescher, A. 1993. Shear bands in biaxial tests on dry coarse sand. *Soils and Foundations*, 33(1), 118–132.

Lade, P.V., Nam, J. and Hong, W.P., 2008. Shear banding and cross-anisotropic behavior observed in laboratory sand tests with stress rotation. *Canadian Geotechnical Journal*, 45(1), 74–84.

Liu, J., 2018. *Numerical investigations of the strain localization in geotechnical engineering within the framework of micropolar theory*. Ph.D. Thesis, École centrale de Nantes.

Liu, J., Wu, L., Yin, K., Song, C., Bian, X. and Li, S., 2022. Methods for solving finite element mesh-dependency problems in geotechnical engineering—a review. *Sustainability*, 14, 2982.

Oda, M., Kazama, H. and Konishi, J., 1998. Effects of induced anisotropy on the development of shear bands in granular materials. *Mechanics of Materials*, 28(1–4), 103–111.

Salgado, R., Bandini, P. and Karim, A., 2000. Shear strength and stiffness of silty sand. *Journal of Geotechnical and Geoenvironmental Engineering*, 126(5), 451–462.

Stefanou, I. and Gerolymatou, E., 2019. Strain localization in geomaterials and regularization: Rate-dependency, higher order continuum theories and multi-physics. *ALERT Doctoral School*, 780, 47–85.

Tang, H., Du, T. and Shao, L., 2018. A plane strain testing apparatus characterized by flexible loading and noncontact deformation measurement and its application to the study of shear band failure of sand. *International Journal of Distributed Sensor Networks*, 14(9).

Tatsuoka, F., Nakamura, S., Huang, C.C., and Tani, K. 1990. Strength anisotropy and shear band direction in plane strain tests of sand. *Soils and Foundations*, 30(1), 35–54.